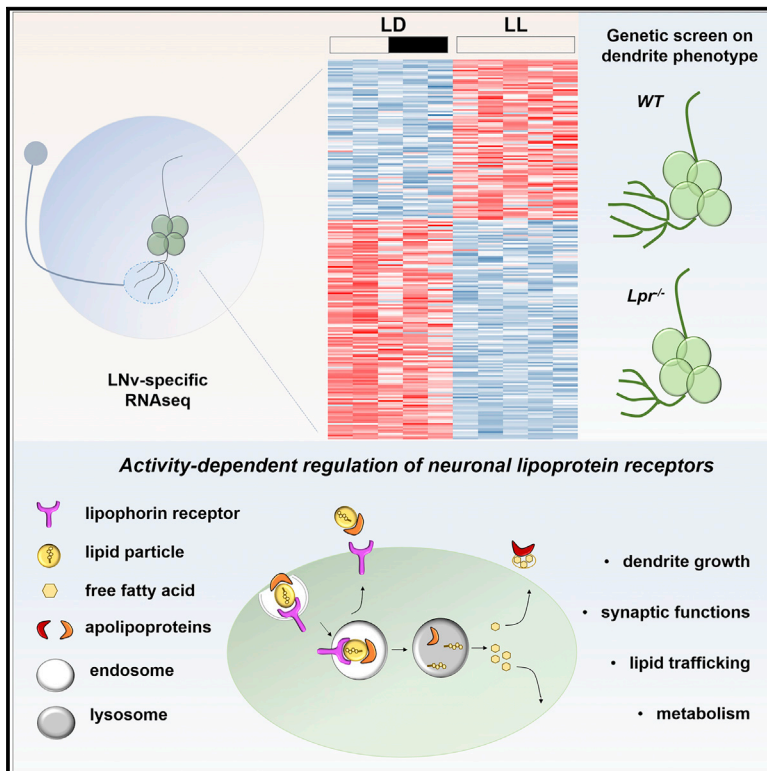# Transcriptional Regulation of Lipophorin Receptors Supports Neuronal Adaptation to Chronic Elevations of Activity

Graphical Abstract

Authors

Jun Yin, Mary Gibbs, Caixia Long, ..., Peng Ding, Uzma Javed, Quan Yuan

Correspondence

quan.yuan@nih.gov

In Brief

Yin et al. highlight *Drosophila* lipophorin receptors (LpRs) as molecular targets for activity-dependent transcriptional regulation and reveal the functional significance of cell-type-specific regulation of neuronal lipid uptake in experience-dependent plasticity and adaptive responses.

Highlights

- Cell-type-specific RNA-seq analyses identify activity modified transcripts

- Activity induces the upregulation of LpR1 and LpR2 transcripts in larval LNvs

- LpRs are required for LNv dendrite morphogenesis during development

- Upregulation of LpRs supports neuronal adaptation to elevated activity

Article

Transcriptional Regulation of Lipophorin Receptors Supports Neuronal Adaptation to Chronic Elevations of Activity

Jun Yin,[1] Mary Gibbs,[1] Caixia Long,[1] Justin Rosenthal,[1] Hyong S. Kim,[1] Anna Kim,[1] Chengyu Sheng,[1] Peng Ding,[2] Uzma Javed,[1] and Quan Yuan[1,3,*]
[1]Dendrite Morphogenesis and Plasticity Unit, National Institute of Neurological Disorders and Stroke, NIH, Bethesda, MD 20892, USA
[2]Neurobiology Department, University of Massachusetts Medical School, Worcester, MA 01605, USA
[3]Lead Contact
*Correspondence: quan.yuan@nih.gov
https://doi.org/10.1016/j.celrep.2018.10.016

SUMMARY

Activity-dependent modifications strongly influence neural development. However, molecular programs underlying their context and circuit-specific effects are not well understood. To study global transcriptional changes associated with chronic elevation of synaptic activity, we performed cell-type-specific transcriptome profiling of *Drosophila* ventral lateral neurons (LNvs) in the developing visual circuit and identified activity-modified transcripts that are enriched in neuron morphogenesis, circadian regulation, and lipid metabolism and trafficking. Using bioinformatics and genetic analyses, we validated activity-induced isoform-specific upregulation of *Drosophila* lipophorin receptors LpR1 and LpR2, the homologs of mammalian low-density lipoprotein receptor (LDLR) family proteins. Furthermore, our morphological and physiological studies uncovered critical functions of neuronal lipophorin receptors (LpRs) in maintaining the structural and functional integrities in neurons challenged by chronic elevations of activity. Together, our findings identify LpRs as molecular targets for activity-dependent transcriptional regulation and reveal the functional significance of cell-type-specific regulation of neuronal lipid uptake in experience-dependent plasticity and adaptive responses.

INTRODUCTION

Sensory experience interacts with genetic programs to shape neuronal connectivity during development. Dendrites receive and integrate sensory signals and synaptic inputs, in turn regulating the growth, patterning, and maintenance of dendritic arbors (Cline and Haas, 2008; Wong and Ghosh, 2002). Studies over the past few decades have demonstrated the ubiquitous yet complex effects elicited by sensory experience on the developing nervous system and have revealed a variety of cellular mechanisms involved in activity-dependent dendrite plasticity

(Dong et al., 2015; Jan and Jan, 2010; Yin and Yuan, 2015). For example, visual stimuli promote dendrite growth in *Xenopus* tectal neurons (Sin et al., 2002). In mammalian olfactory mitral cells and retinal ganglion cells, activity-dependent dendritic remodeling is critical for the proper establishment of connectivity during circuit maturation (Malun and Brunjes, 1996; Wang et al., 2001). Sensory experience also impacts mammalian cortical development by regulating the maturation rate and dendrite growth in inhibitory neurons (Chattopadhyaya et al., 2004; Mardinly et al., 2016). In contrast to the advanced understanding of cellular mechanisms, molecular machinery underlying dendrite plasticity remains largely uncharacterized. Current knowledge on this topic is limited to the calcium-related signaling events mediated via either voltage-gated calcium channels (VGCCs) or neurotransmitter receptors (Flavell and Greenberg, 2008; Lohmann and Wong, 2005).

To achieve a better understanding of molecular programs mediating activity-induced responses of the developing CNS, recent efforts have been directed toward circuitry and context-specific studies. Cell-type-specific transcriptome analysis is a powerful approach for analyzing global changes of molecular programs induced by sensory experience and neuronal activity. RNA sequencing (RNA-seq) analyses of both mammalian cortical neurons and *Drosophila* CNS neurons have demonstrated activity-dependent transcriptional inductions of cell-type-specific gene programs, which are functionally important for a coordinated adaptive response generated by individual components within a neural circuit (Chen et al., 2016; Malik et al., 2014; Spiegel et al., 2014).

Using *Drosophila* ventral lateral neurons (LNvs) as a model, we combined cell-type-specific transcriptome analyses and genetic studies to identify genes with experience-modified transcriptional profiles and functions in regulating dendrite development and plasticity. LNvs exhibit experience-dependent homeostatic regulation of dendrite growth in response to chronic alterations of visual input (Yuan et al., 2011). By comparing the LNv transcriptome profiles obtained from constant light versus regular light and dark conditions, we identified 230 DE transcripts that are enriched in genes related to neuronal morphogenesis, circadian regulation, and lipid metabolism and trafficking, among which *Drosophila* lipophorin receptors (LpRs) were identified as top candidates by bioinformatics and genetic analyses.

Similar to their mammalian homologs, the low-density lipoprotein receptor (LDLR) family proteins, *Drosophila* LpRs mediate lipid uptake in peripheral tissues, but have not been characterized in neurons (Parra-Peralbo and Culi, 2011; Rodríguez-Vázquez et al., 2015). Our analyses validated the activity-induced upregulation of LpRs in LNvs at both the transcript and protein levels and demonstrated critical functions of *Drosophila* LpRs in supplying lipids for dendrite development and in maintaining synaptic functions in LNvs experiencing chronic elevations of input activity.

Taken together, our studies provide *in vivo* evidence for the activity-dependent transcriptional regulation of neuronal lipoprotein receptors, a mechanism for augmenting the capacity of lipoprotein uptake in response to alterations of synaptic activity. Given the importance of lipid homeostasis in the development and maintenance of neuronal structure and function, as well as the evolutionarily conserved molecular machinery involved in its regulation (Bailey et al., 2015; Meltzer et al., 2017; Welte, 2015), our findings provide a set of molecular targets for studies related to neuronal adaptive responses and have important implications in both neural development and neurodegeneration.

RESULTS

Cell-Type-Specific Transcriptome Profiling for Identification of Visual-Experience-Modified Transcripts in LNvs

Drosophila larvae sense light through the Bolwig's organ (BO), which sends axonal projections via the Bolwig's nerve (BN) into the larval optic neuropil (LON) and makes synaptic contact with the dendritic arbors of LNvs (Sprecher et al., 2011; Yuan et al., 2011). LNv dendrites exhibit visual-experience-dependent structural plasticity. During development, larvae receiving chronically elevated visual inputs through constant light exposure (LL) show reduced LNv dendrite size as compared to larvae raised under standard light/dark (12:12) (LD) conditions (Figure 1A; Yuan et al., 2011). To understand the molecular program underlying this sensory experience-induced change in dendrite morphogenesis, we performed cell-type-specific transcriptome sequencing using LNvs collected from larvae cultured in LL and LD conditions.

There are four LNvs in each brain lobe that are specifically labeled by the expression of GFP driven by the Pdf promoter (Figure 1A; Malpel et al., 2002; Yuan et al., 2011). To construct LNv-specific RNA-seq libraries, we used fluorescence-activated cell sorting (FACS) to isolate GFP-labeled LNvs from dissociated larval brains and then generated five libraries for each condition (Figures S1A and S1B). Among the total mapped reads, 30%–50% were mapped to mRNAs, 40%–50% were mapped to rRNAs, and the other 10% were shared by other types of RNAs. In total, we detected mRNAs of 5,000–7,000 genes for each condition (Figures S1C and S1D).

We first performed a Pearson's correlation analysis of the raw mRNA reads to assess the variance of the transcriptome sequencing results. The correlation coefficients of five biological replicates within LD or LL groups were high, ranging from 0.9 to 1, while coefficients were lower between LD and LL

groups, ranging from 0.8 to 0.9 (Figure 1B). The overall correlation (>80%) indicates the high reproducibility among individual RNA-seq libraries. In addition, principal-component analysis (PCA) of all biological repeats shows that the LD and LL samples were separated into distinct clusters, confirming the consistency within the same conditions and detectable separation between LD and LL conditions (Figure 1C).

To assess the quality of our RNA-seq libraries, we compared the expression levels of a subset of genes in libraries generated using either dissociated LNvs or whole larval brains (Figure S2). Notably, pigment-dispersing factor (PDF), a signature neuropeptide expressed specifically in LNvs, showed the highest expression level of all mRNAs in our LNv libraries (Figures 1D and S2). Other genes previously identified to be enriched in LNvs were also enriched in our libraries, including *Pdfr*, the PDF receptor; *Fer2*, a transcription factor involved in LNv differentiation; and *cry*, a blue-light-sensing photoreceptor. By contrast, two genes with high expression in the larval brain, *mushroom body miniature* (*mbm*), which is involved in mushroom body development, and *EGF-domain O-GlcNAc transferase* (*Eogt*), which is responsible for extracellular O-GlcNacylation, had no detectable expression in our LNv libraries (Figure S2). These data suggest that our RNA-seq libraries preserve the characteristic expression profile of LNvs.

Constant light conditions, besides providing chronic elevation of visual inputs, also modify gene expression profiles in LNvs within the context of circadian regulation (Claridge-Chang et al., 2001; McDonald and Rosbash, 2001). Consistent with this prediction, we detected altered expression levels of major circadian genes, including *Clk*, *sNPF*, *per*, and *tim* (Figures 1D and S3; Darlington et al., 1998; Yu and Hardin, 2006). Our validation processes provide evidence supporting both the consistency and specificity of our RNA-seq analyses.

Identification of Experience-Dependent Transcriptional Changes in LNvs

To identify genes with differential expression profiles in LD versus LL conditions, we performed bioinformatics analyses using the DESeq2 statistics program. To focus on genes with consistently detectable expression in LNvs, we used the DESeq2 autothreshold and analyzed the top 28% of highly expressed genes (Figure 2A). With a false discovery rate (FDR; adjusted p value) of less than 0.1 and a difference in expression level greater than 2 (log2 > 1), 230 genes were detected as differentially expressed (DE) (Figure 2A; Table S1). Of these genes, 97 are upregulated and 133 are downregulated in LNvs (Figure 2B; Table S1).

To determine biological processes or molecular functions that are enriched in the activity-modified transcripts, we performed Gene Ontology (GO) analysis using DAVID bioinformatics resources (https://david.ncifcrf.gov/) (Figure 2C; Table S2; Huang da et al., 2009). In the biological process category, the top enriched clusters include molecules involved in neuron projection morphogenesis, learning and memory, circadian rhythm, cell adhesion, and regulation of synaptogenesis. In the molecular function category, the top enriched clusters contain molecules
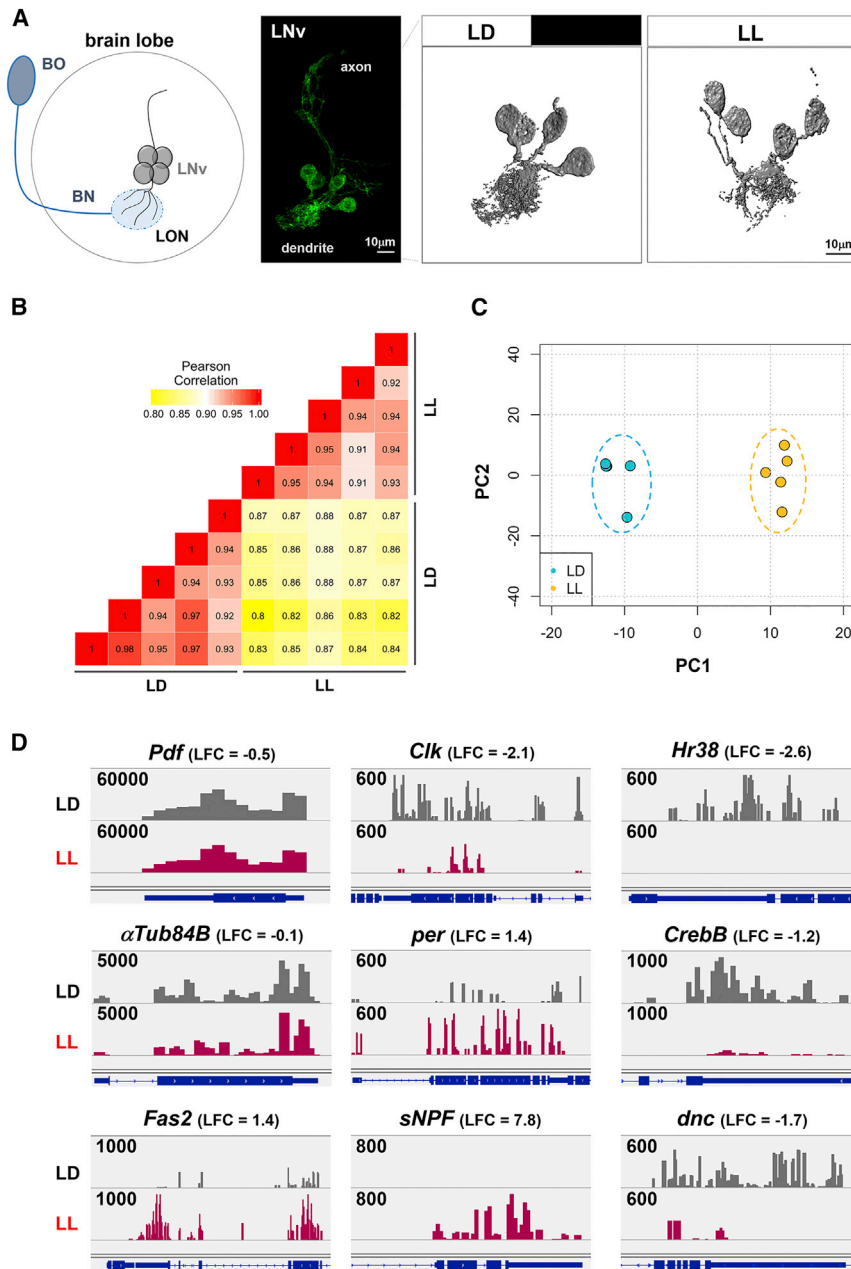
scriptional profiles are distinguishable from circadian-driven oscillations, facilitating our subsequent investigations.

Among the activity-modified transcripts, we detected several genes implicated in the structural or functional plasticity in the *Drosophila* nervous system, including *Fas2*, *dnc*, and *CrebB* (Figure 1D; Sivachenko et al., 2013; Yuan et al., 2011). *Hr38*, a nuclear receptor regulated by neuronal activity, also showed highly differential expression in LD versus LL conditions (Figure 1D; Fujita et al., 2013). In addition, key genes regulating neural morphogenesis, such as *fra*, *NetB*, and *drl*, were among the top DE genes (Figures 2B and 2C; Table S2). These findings are consistent with the notion that sensory experience strongly influences the *Drosophila* developmental program and provided us with candidates for future developmental studies.

To understand potential interactions among these DE genes, we also performed a protein-protein interaction (PPI) network analysis using the NetworkAnalyst tool (http://www.networkanalyst.ca/) (Xia et al., 2015). The PPI network analysis generates a global view of gene networks and pathways through known protein interactions and provided preliminary information regarding the biological relevance of the DE genes. Among the genes in our DE list, we identified 40 upregulated and 54 downregulated genes as seeds (Figures S4A and S4B). Among these

with immunoglobulin-like domains, low-density lipoprotein receptor activity, sequence-specific DNA binding, and amino acid transport functions.

LNvs are the main components of the *Drosophila* circadian circuit. As expected, we found circadian-related genes in our DE gene list. There were 29 and 37 DE genes overlapping with circadian-regulated genes identified from adult LNvs or by the CLOCK chromatin immunoprecipitation sequencing (ChIP-seq) datasets, respectively (Figures S3A and S3B; Abruzzi et al., 2011, 2017). The analysis confirmed global circadian changes of the LNv transcriptome induced by constant light conditions and, more importantly, validated that the activity-modified tran-

A

- up-regulated gene
- down-regulated gene

B

C

highly connected PPI nodes, genes related to metabolism and actin-related cytoskeleton organization were enriched, which is consistent with the findings generated by the GO analysis (Figures S4A and S4B).

Based on our GO and PPI network analyses of the experience-modified transcripts in LNvs, we concluded that cell adhesion molecules, lipoprotein receptors, and transcription factors are potentially the main targets of transcriptional regulation induced by chronic elevations of activity. These enriched categories also indicate that the molecular machineries controlling neuronal morphogenesis and lipid trafficking are strongly influenced by sensory experience during development.

In Vivo RNAi Screen for Candidate Genes Involved in Activity-Dependent Regulation of LNv Dendrite Morphogenesis

Guided by the GO and PPI network analyses, we screened 149 transgenic RNAi lines targeting candidate genes that belong to functional groups including cell adhesion molecules, molecules related to lipid uptake and metabolism, and transcription

factors. RNAi-mediated knockdown of 42 of the 90 candidate genes generated dendrite morphology phenotypes of varying severities (Table S3), suggesting the critical function of activity-dependent transcriptional regulation in LNv dendrite morphogenesis.

In particular, LNv-specific RNAi knockdown of *Drosophila* LpRs *LpR1* and *LpR2*, as well as *SREBP*, a transcriptional factor regulating LpR2 expression (Sieber and Spradling, 2015), and *schlank*, a ceramide synthase functioning upstream of SREBP (Bauer et al., 2009), all led to clear dendrite reduction phenotypes, while the axonal projection of LNvs were largely unaffected (Figures 3A, 3C, and S5; Table S4). The genes in this set belong to the same signaling pathway regulating lipoprotein synthesis, transport, and metabolism, with the LpRs being the downstream targets. Our RNA-seq analyses showed elevated levels of both LpRs and *schlank* transcripts in LL conditions, although there was no change in SREBP, which is known to be regulated through posttranscriptional proteolytic processing and translocation activation (Figure 3B; Horton et al., 2002). Notably, *LpR1* was among the top 10 upregulated genes found by both DEseq2 (Figure 2B) and the PPI network analysis (Figure S4A). Based on the combined results from the morphological screen and RNA-seq analysis, we focused on the LpRs in the follow-up analyses.

Activity-Induced Upregulation of *LpR1* and *LpR2* Transcripts in LNvs

Drosophila LpR1 and *LpR2* are located in tandem on the 3rd chromosome and have 61% identity in their protein sequences. They are transmembrane receptors sharing signature functional domains with the mammalian LDLR family proteins, including LDLR receptor type A modules (LA), epidermal growth factor
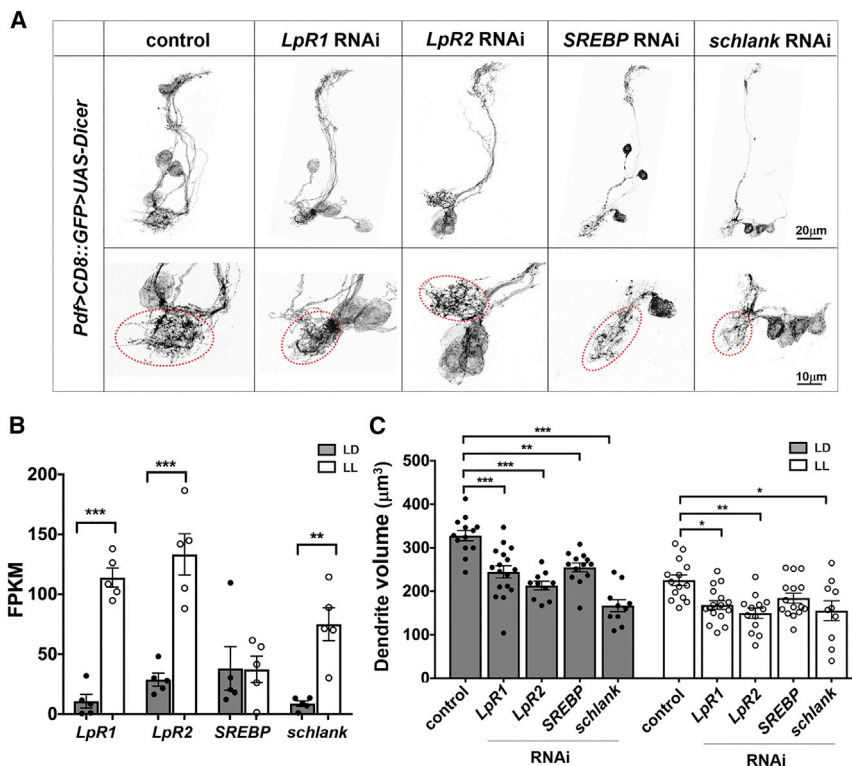
A

B

C

(EGF) modules, and YWTD β-propellers. Intriguingly, multiple isoforms of LpR1 and LpR2 were detected in *Drosophila* cDNAs with distinct tissue distributions and properties (Parra-Peralbo and Culi, 2011; Rodríguez-Vázquez et al., 2015).

Through exon mapping of LNv-specific RNA-seq data, we examined specific isoforms of *LpRs* expressed in LNvs. Reads corresponding to exons encoding the long isoforms for both receptors (exons 1–4 for *LpR1* and 1–3 for *LpR2*) were absent from LNv-specific libraries, suggesting that LNvs only express short isoforms of LpRs. In contrast, reads corresponding to exons encoding multiple short isoforms of *LpR1* and *LpR2* were detected in LNv libraries (Figure S7B; Tables S5 and S6).

To validate the activity-induced upregulation of LpR transcripts in LL, we performed quantitative fluorescent *in situ* hybridization (qFISH) on acutely dissociated LNvs using an *LpR2*-specific probe (Figure S6A). We observed the expression of *LpR2* in LNvs and a significant increase in *LpR2* transcript levels induced by LL conditions (Figure 4A).

Previous studies and our RNA-seq analyses indicate that besides influencing activity-dependent transcriptional programs, LL conditions also modify many circadian regulated transcripts (Figure S3; Claridge-Chang et al., 2001; McDonald and Rosbash, 2001). To confirm that the increase in *LpR2* expression in LL is driven by the activity-dependent mechanism and not by circadian rhythm, we performed qFISH experiments in wild-type larvae at two different circadian time points, ZT2 and ZT14, 2 hr into the subjective day and night, respectively, as well as in the *per⁰* mutant, which is arrhythmic due to the loss-of-function mutation in the core clock component *period* (Figures 4B and 4C).

In wild-type larvae, qFISH studies on *LpR2* indicated that there is no significant difference between samples collected at ZT2 and ZT14 (Figure 4B), suggesting that *LpR2* transcription is not regulated by circadian rhythm. Consistently, we also observed elevated levels of *LpR2* transcripts in *per⁰* mutant larvae cultured under the LL condition, as compared to the LD condition (Figure 4C). Both results strongly support that LL-induced upregulation of *LpR2* transcripts is activity dependent and does not rely on a functional circadian system.

LL Elevates the Protein Level of LpR2 in LNvs

To examine the expression level of LpR2 protein specifically in LNvs, we used the MiMIC-LpR2-RMCE line that expresses a LpR2-EGFP fusion protein (LpR2-EGFP[MI04745]) generated by the *in vivo* protein tagging approach (Nagarkar-Jaiswal et al., 2015). The RMCE (recombinase-mediated cassette exchange) cassette containing an EGFP coding sequence was targeted to the region between LpR2 exons 12 and 13 using the Minos-mediated integration technique, and the resulting fusion protein represents both the long and short isoforms of LpR2 (Figure 5A). This *in vivo* tagging approach allows LpR2-EGFP[MI04745] to be expressed at the native locus, likely reflecting the endogenous LpR2 expression level and distribution.

In the larval CNS, we observed LpR2-EGFP[MI04745] signals in many neurons, including LNvs (Figures 5B and S6B). We quantified EGFP intensity within the somatic regions of LNvs and found a significant increase of LpR2-EGFP[MI04745] expression in LL compared to LD conditions (Figures 5C and 5D). This result indicates that the protein level of LpR2 in LNvs is also modified by the LL condition, consistent with the transcriptional upregulation revealed by our RNA-seq analysis.
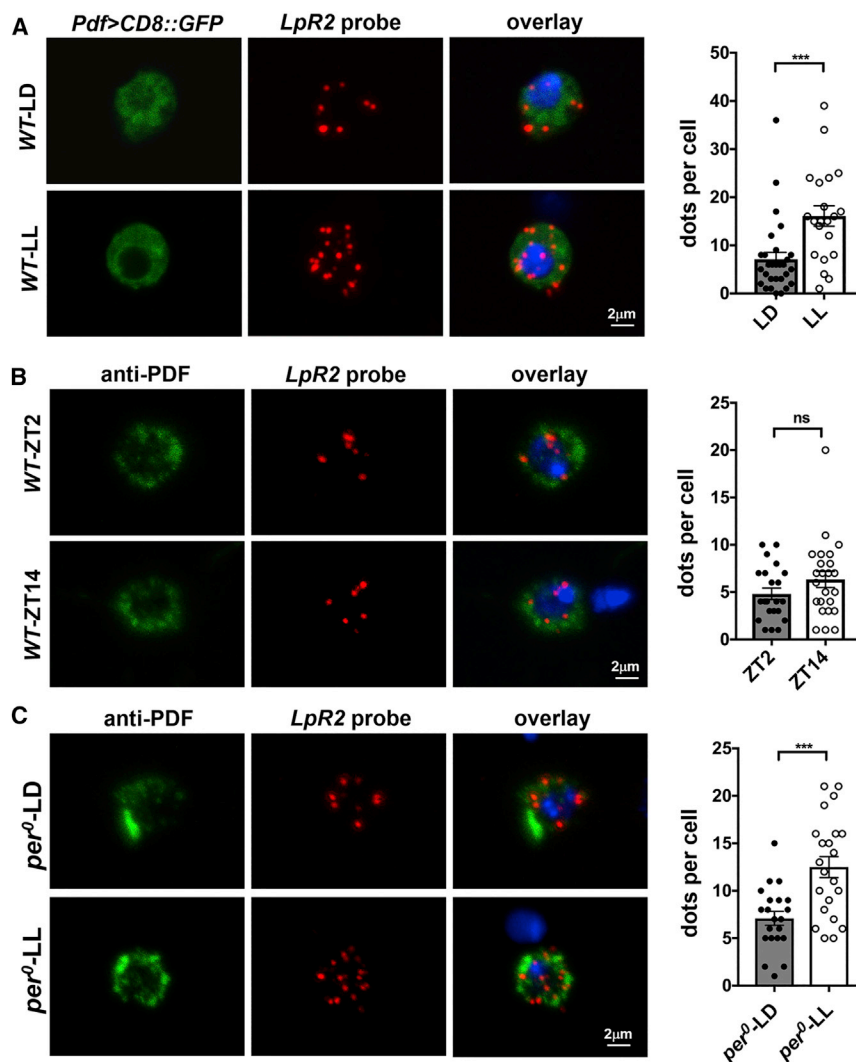
Figure 4. Activity-Induced Upregulation of LpR2 Transcripts in LNvs

(A) The LL-induced upregulation of *LpR2* transcripts was validated by qFISH experiments using an *LpR2*-specific probe in dissociated LNvs from 3rd-instar larvae brains. Left: representative projected confocal images of single LNvs labeled by a *Pdf* enhancer driving CD8::GFP (green), the *LpR2* probe (red dots), and DAPI (blue). Right: the number of dots generated by the *LpR2* probe in LNv somas was quantified, revealing a significant increase in *LpR2* transcript levels induced by LL conditions. n represents the number of dissociated LNvs. n = 21–29 in all groups.

(B) No significant difference in *LpR2* transcripts was detected between LNvs collected at circadian time points ZT2 and ZT14. LNvs were labeled by anti-PDF staining (green), the *LpR2* probe (red dots), and DAPI (blue). n = 22–24 in all groups.

(C) The LL-induced upregulation of *LpR2* transcripts was also detected in the circadian mutant per^0. LNvs were labeled by anti-PDF staining (green), the *LpR2* probe (red dots), and DAPI (blue). n = 22–24.

Statistically significant differences were determined by Student's t test. ns, not significant; ***p < 0.001. Error bars represent mean ± SEM.

ing that LpRs are cell-autonomously required for LNv dendrite development. However, the size of LNv dendrites in LL conditions is reduced, while the level of LpRs is high. These observations suggest that LL-induced upregulation of LpRs is not responsible for the activity-induced reduction in LNv dendrite size. Rather, the elevated levels of LpRs likely reflect increased demands for lipoprotein trafficking and serve as a part of the compensatory responses for neurons to adapt to chronic elevation of input activity.

We observed puncta-like LpR2-EGFP[MI04745] signals localized in both LNv dendrites and somatic regions (Figure 5B). To examine LpR2's intracellular localization at high resolution, we performed immunohistochemical studies on a hemagglutinin (HA)-tagged LpR2 transgene, which specifically expresses a short isoform of LpR2 (LpR2F-HA) in LNvs (Parra-Peralbo and Culi, 2011; Soukup et al., 2009). Both the mammalian LDLR and LpRs of other insect species uptake lipids through endocytosis (Brown and Goldstein, 1976; Van Hoof et al., 2005). In larval LNvs, we also observed that Rab5-GFP, an early endosome marker (Entchev et al., 2000), and LpR2F-HA largely colocalize within vesicles in both somas and dendritic arbors of LNvs (Figure 5E). The endosomal localization of the short isoform of LpR2 protein suggests that the *Drosophila* LpRs are likely endocytic receptors for lipoproteins in larval CNS neurons.

LpRs Are Required for Dendrite Morphogenesis during Development

RNAi knockdown of either LpRs or their upstream regulators generates consistent dendrite reduction phenotypes, suggest-

To test this model and elucidate the neuronal functions of LpRs, we performed genetic studies and examined LNv dendrite phenotypes in three loss-of-function mutants of LpRs (Parra-Peralbo and Culi, 2011). All mutants exhibited significant reductions in dendrite volume in both LD and LL conditions, with the most severe phenotype observed in LpR1/2$^{-/-}$ double mutants (Figures 6A–6C), similar to the results obtained through the LNv-specific RNAi knockdown approach. We then performed genetic rescue experiments by specifically expressing LpR1D and LpR2F, the short isoforms of LpRs, in LNvs and examining the dendrite phenotypes in both mutant and wild-type backgrounds (Parra-Peralbo and Culi, 2011; Rodríguez-Vázquez et al., 2015).

While expressing both short isoforms of LpRs in the wild-type background did not generate significant changes in LNv dendrite morphology, the LNv-specific expression of LpR2F largely rescued *LpR2* mutant phenotypes, with the dendrite volume resembling the wild-type control (Figures 6D and 6E) and supporting the cell-autonomous function of the short-isoform
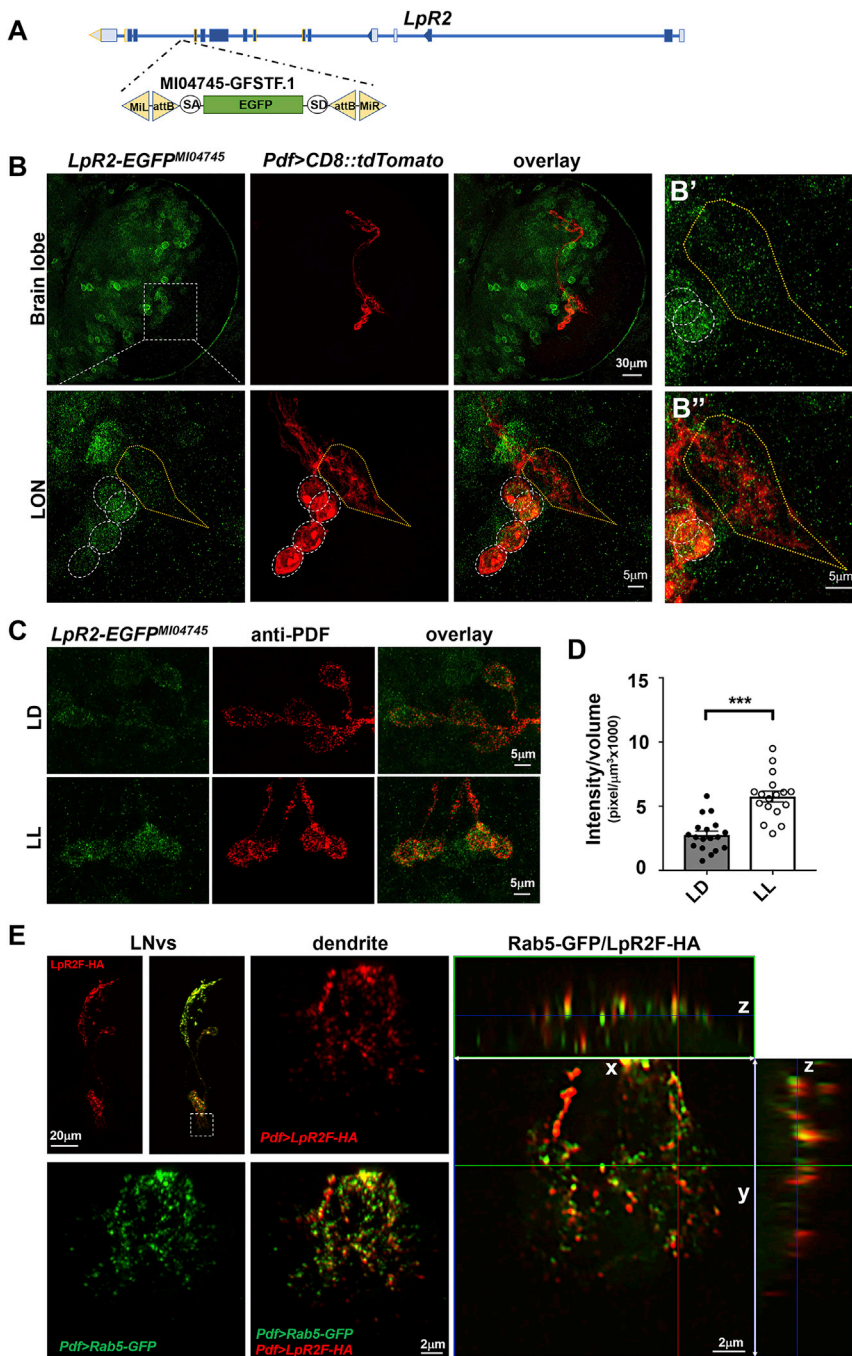
Figure 5. Chronic Elevations of Activity Upregulate LpR2 Proteins in LNvs

(A) The MiMIC-LpR2-RMCE line that expresses a LpR2-EGFP fusion protein (LpR2-EGFP^{MI04745}) potentially reflects endogenous LpR2 expression. Schematic of the MiMIC-based *in vivo* EGFP tagging for LpR2 is shown.

(B) LpR2-EGFP^{MI04745} broadly expresses in the 3rd-instar larval brain and in LNvs. Representative projected confocal images of LNvs labeled by LpR2-EGFP^{MI04745} (green) and *Pdf-LexA* driving LexAop-tdTomato (red) are shown. Somas (white circles) and dendritic regions (yellow frame) are shown in the zoomed-in images (right panels, B′ and B″).

(C) LpR2 protein levels are increased in LL compared to LD conditions. LNvs were labeled by anti-PDF antibody (red) and LpR2-EGFP^{MI04745} (green).

(D) Quantification of the relative intensity of LpR2-EGFP^{MI04745} signals in LNv somas. Statistically significant differences were determined by the Student's t test. ***p < 0.001. Error bars represent mean ± SEM; n = 17–18.

(E) Colocalization of an HA-tagged short isoform of LpR2 (LpR2F-HA) (red) with the endosome marker Rab5-GFP (green) in LNvs. Left: representative projected confocal images of the LNv neuron and zoomed-in images of the LNv dendritic region (white square) are shown. Right: a single optic section with the x-y-z axes, illustrating the colocalization of the LpR2F-HA signals with Rab5-GFP.

for LNv dendrite morphogenesis during development. In addition, the overexpression studies as well as the LpR1D rescue experiment both suggest that an elevated level of LpRs alone is not sufficient to alter the size of LNv dendrites. These findings are consistent with our model, in which LpRs are upregulated as a part of the compensatory response for neurons to adapt to chronically elevated activity.

Experience-Dependent Upregulation of LpRs Is Important for Maintaining the Functional Properties of LNvs

To further investigate the functional significance of the activity-induced upregulation of LpRs, we performed physiological studies in LNvs using calcium imaging experiments with a genetically encoded calcium indicator, GCaMP6s (Yuan et al., 2011). By subjecting larval eye-brain preparations to light stimulations, we observed light-elicited physiological responses in LNvs, which can be quantified by increases in GCaMP signals recorded at the axonal terminal regions (Figures 7A–7D).

Using this approach, we found that light-induced calcium responses in LNvs were consistently dampened by *LpR1* or *LpR2* RNAi knockdown (Figures 7B–7D). Importantly, compared

LpR2 in regulating LNv dendrite growth. In contrast, the LpR1D transgene failed to rescue the dendrite defects in *LpR1* mutants. Based on the exon mapping results from our RNA-seq analysis (Figure S7; Tables S5 and S6), there are multiple short-isoform transcripts of *LpR1* and *LpR2* detected in the LNvs. It is possible that the expression of LpR1D isoform alone is not sufficient to reconstitute the function of LpR1 in LNvs.

Together, the RNAi knockdown and mutant rescue experiments demonstrate the cell-autonomous requirement of LpRs
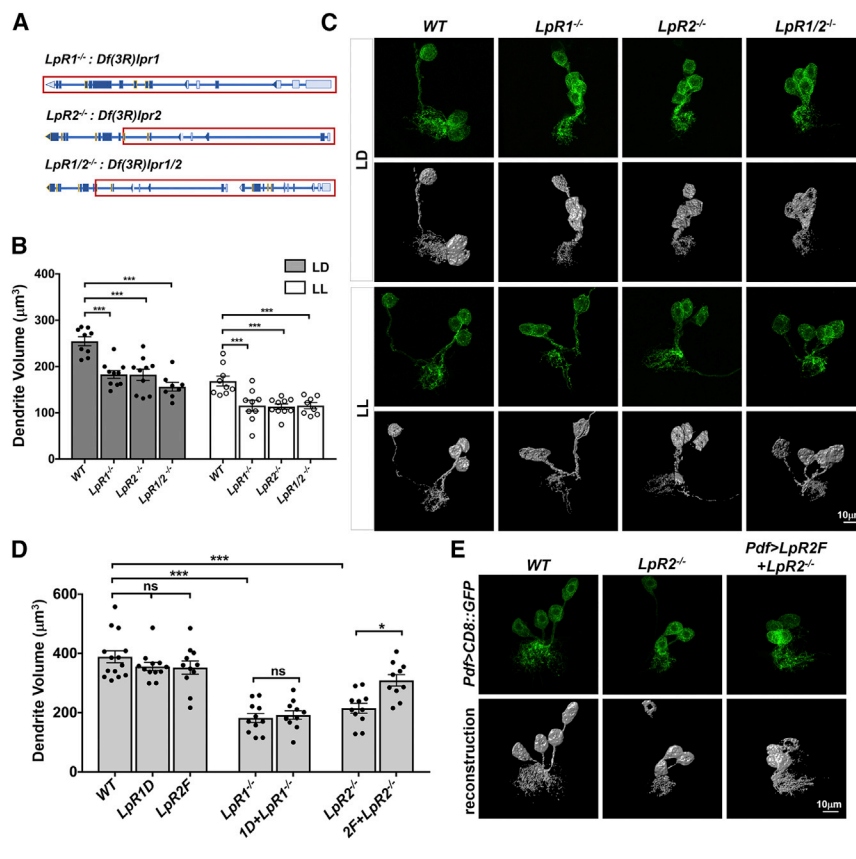
Figure 6. LpRs Are Required for Dendrite Morphogenesis during Development

(A–C) LpRs are required for LNv dendrite morphogenesis.

(A) Schematics showing the deleted genomic regions (red) in the null mutants of *LpR1*, *LpR2*, and the *LpR1/2* double mutant.

(B) LNv dendrite volumes are significantly reduced in lipophorin receptor (*LpR*) mutants. Quantification of LNv dendrite volume for controls and *LpR* mutants in LD and LL conditions is shown. LNv morphology is marked by the *Pdf* enhancer driving CD8::GFP expression. Statistical differences were determined by one-way ANOVA followed by Tukey post hoc test. *p < 0.05; **p < 0.01; ***p < 0.001. Error bars represent mean ± SEM; n = 8–10.

(C) Representative projected confocal images (green, top panels) and 3D volume reconstructions (gray, bottom panels) of LNv somas and dendritic regions are shown.

(D and E) Overexpression of short isoforms of LpRs and genetic rescue of LNv dendrite phenotypes in *LpR1*$^{-/-}$ and *LpR2*$^{-/-}$ mutants.

(D) Quantification of LNv dendrite volumes in controls and *LpR* mutants collected in LD conditions is shown. Expression of LpR2F in LNvs rescues the *LpR2* mutant phenotype, while expression of LpR1D does not rescue the *LpR1* mutant phenotype. Pdf-Gal4 driving UAS-CD8::GFP, together with either UAS-LpR1D or UAS-LpR2F transgenes, was tested in the wild-type or mutant backgrounds. Statistically significant differences were determined by one-way ANOVA followed by Tukey post hoc test. ns, no significance, *p < 0.05, ***p < 0.001. Error bars represent mean ± SEM; n = 10–14.

(E) Representative projected confocal images of LNv somas and dendritic regions are shown for the genetic rescue of *LpR2* mutants by the LNv-specific expression of an LpR2F transgene.

to LNvs in the LD condition, where either *LpR1* or *LpR2* knockdown produced a moderate reduction in the light response, LNvs in LL conditions appeared to be affected by *LpR* knockdown to a much larger degree and showed significantly reduced calcium responses to light stimulation. This result reveals that besides supporting dendrite morphogenesis during development, LpRs are also essential for maintaining physiological responses and synaptic functions in neurons challenged with chronic elevations of activity, strongly indicating the LL-induced upregulation of LpRs as a part of the compensatory response that counteracts the activity-induced morphological and functional alterations.

DISCUSSION

In this study, we investigated experience-dependent regulation of dendrite plasticity using cell-type-specific transcriptome profiling followed by transgenic RNAi screens. We identified candidate genes that are subject to activity-dependent transcriptional regulation and function in regulating dendrite development in the *Drosophila* CNS. Additionally, combined bioinformatics and genetic analyses revealed isoform-specific expression of lipoprotein receptors LpR1 and LpR2 in LNvs

and uncovered their roles in supporting dendrite morphogenesis and synaptic functions in the CNS. Together, our findings provide *in vivo* evidence for neuronal lipoprotein receptors serving as targets of activity-dependent transcriptional regulation, a previously unrecognized component of the neuronal homeostatic mechanism that maintains structural and functional integrity in response to chronic elevation of input activity.

Identification of Molecular Targets of Activity-Dependent Regulation

Activity-dependent transcriptional factors serve important functions in synapse development, maturation, and elimination as well as dendritic and axonal outgrowth (Cohen and Greenberg, 2008; Dijkhuizen and Ghosh, 2005; Flavell and Greenberg, 2008). However, a molecular understanding of circuit and context-specific transcriptional events induced by sensory experience is just starting to emerge (Abruzzi et al., 2017; Chen et al., 2016; Malik et al., 2014). Our cell-type-specific RNA-seq analyses identified over 200 experience-modified transcripts, among which are previously identified activity-dependent genes, including *CrebB*, *Hr38*, *dnc*, and *Irk1*, as well as many candidate genes that have not been previously linked to activity-dependent regulation or been functionally characterized
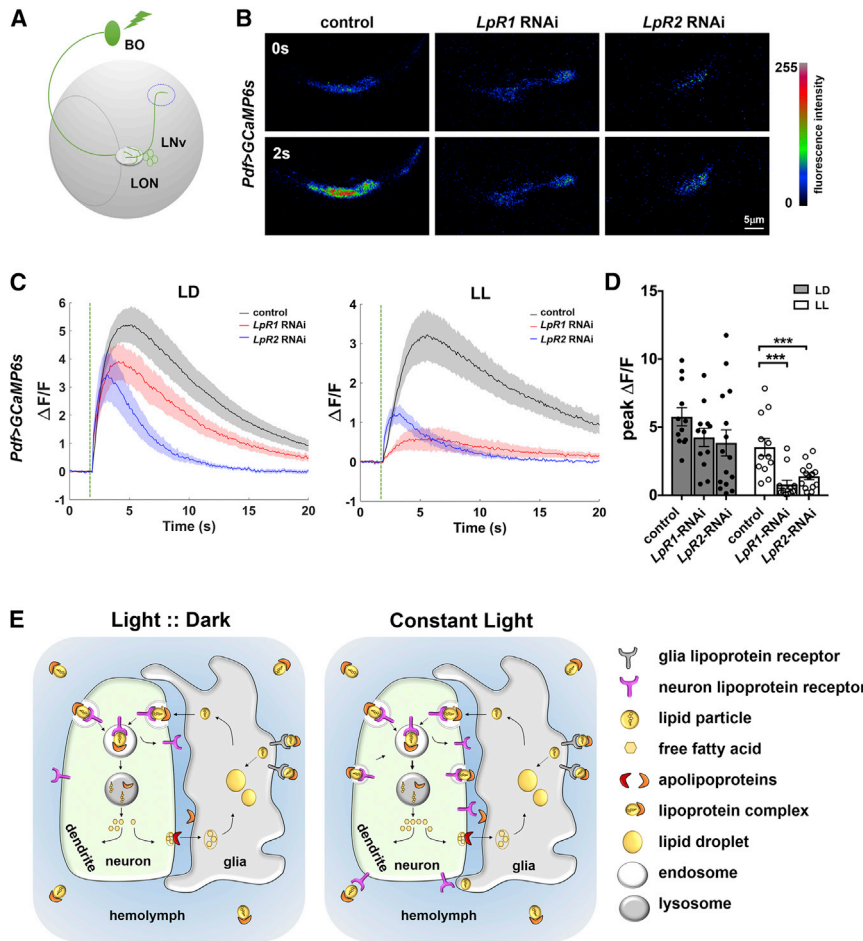
Figure 7. LpRs Are Required for Supporting Functional Properties of LNvs Challenged by Chronically Elevated Activity

(A) The schematic diagram illustrating the setup for calcium imaging experiments in LNvs. The light pulse elicits calcium responses in LNvs, which are recorded at the axonal terminal region (dashed blue circle).

(B) Representative frames of the *Pdf > GCaMP6s* recordings at 0 and 2 s after stimulation for control and *LpR* RNAi knockdown in the LL condition.

(C) Light-elicited calcium responses in LNvs are severely affected by *LpR RNAi* knockdown in the LL condition. The traces show the average GCaMP signals recorded at the axonal terminal region in LNvs. The shaded area represents SEM. Genotypes and culture conditions are as indicated. The dashed green line represents the light stimulation delivered by a 100-ms light pulse.

(D) The quantifications of peak value of the changes in GCaMP signal induced by light stimulations (ΔF/F). Statistics by one-way ANOVA followed by Tukey post hoc test. ***$p < 0.001$. Error bars represent mean ± SEM; n = 12–15.

(E) The proposed model for activity-dependent regulation of LpRs serving as a compensatory mechanism to augment the capacity for neuronal lipoprotein uptake in response to chronic elevation of input activity. LpRs recruit lipoprotein complexes through neuron-glia interactions or by capturing lipophorins in the circulating hemolymph. Constant light conditions generate increased lipid demand and the subsequent up-regulation of the neuronal LpRs required for increased lipid uptake, an important mechanism for maintaining the normal morphology and synaptic functions of the neuron.

in neurons. Therefore, our study generated a large number of potential targets for future molecular studies on experience-dependent dendrite plasticity. Besides the list of activity-modified transcripts, our analyses also revealed isoform-specific regulation of LpR genes, demonstrating the possibility of studying alternative splicing events associated with chronic alterations of activity using our RNA-seq dataset.

Isoform-Specific Transcriptional Regulation of LpRs Generates Functional Diversity

Both insect LpRs and mammalian LDLR family proteins have multiple isoforms generated by alternative splicing events and the usage of alternative promoters (Ling et al., 2010; Magrané et al., 1999; May et al., 2003; Parra-Peralbo and Culi, 2011). In the fly imaginal disc and oocyte, long isoforms of LpRs acquire their lipoprotein cargo by interacting with lipid transfer particles (LTP), which stabilize the receptor-lipoprotein complex on the cell surface and possibly facilitate lipolysis (Parra-Peralbo and Culi, 2011; Rodríguez-Vázquez et al., 2015). In these non-neuronal tissues, long isoforms of LpRs are also solely responsible for endocytosis-independent neutral lipid uptake. The function of the short isoforms, however, is unclear. When overexpressed in imaginal discs, the short isoform of LpR2 localizes in

early endosomes and mediates uptake of lipoproteins through endocytic activities similar to those observed in mammalian LDLRs (Parra-Peralbo and Culi, 2011; Rodríguez-Vázquez et al., 2015; Van Hoof et al., 2005). These observations suggest that isoform-specific transcriptional regulation generates LpRs with diverse properties and functionalities.

Our studies in LNvs indicate that the short-isoform of LpR2 has an endosomal localization in neurons and the ability to reconstitute LpR2 function in supporting dendrite growth (Figures 5E, 6D, and 6E). In conjunction with previous studies, our results suggest that isoform-specific transcriptional regulation may lead to distinct modes of lipoprotein intake in cells expressing different isoforms. We propose that the short isoforms of LpR1 and LpR2 expressed in neurons are endocytic lipoprotein receptors responsible for neuronal lipid uptake. In the CNS, lipid trafficking and homeostasis involve neural-glia interactions, which likely alter local concentrations of lipoprotein complexes and generate unique demands for lipoprotein uptake compared to non-neuronal tissues (Liu et al., 2015, 2017; Palm et al., 2012). Future *in vivo* imaging studies on CNS lipoprotein trafficking combined with functional studies of different LpR isoforms will contribute to our understanding of the molecular regulation of neuronal lipid uptake.

Neuronal Lipid Uptake Contributes to the Maintenance of Lipid Homeostasis in the CNS and Is an Important Component of Compensatory Responses to Elevated Neuronal Activity

Lipids are essential building blocks for plasma membranes and vesicles. They also have versatile roles in regulating cellular metabolism and mediating signaling transductions. In the nervous system, neuronal lipid uptake and recycling involve complex neuron-glia interactions that are critical for lipid homeostasis in the brain (Bruce et al., 2017; Hayashi, 2011; Walther and Farese, 2012). Although neurons have the intrinsic ability to synthesize lipids, glia-derived cholesterol and phospholipids are essential for the formation and maintenance of the synapse in mammalian CNS neurons (Mauch et al., 2001). Recent studies in the *Drosophila* system also demonstrated that glial lipid droplet formation protects neural stem cells from systematic stress in the developing *Drosophila* larval brain (Bailey et al., 2015) and that the inability of neurons to transport lipids for glial lipid droplet formation leads to accelerated neurodegeneration (Liu et al., 2017). However, whether and how neuronal lipid uptake contributes to normal development and activity-induced plasticity events remain unknown.

Our studies demonstrate the function of LpRs in supporting dendrite growth. Reducing or eliminating LpRs in LNvs leads to a significant decrease in dendrite volume. Counterintuitively, LpRs are upregulated in LL conditions, which also generate reductions in LNv dendrite volume. Although an increased LpR level in the LL condition does not increase dendrite size, it is critical for preventing a further reduction in dendrites and a loss of physiological functions, suggesting that LpRs counteract activity-induced morphological and functional alterations. Based on these observations and current knowledge of lipid homeostasis in the larval CNS, we propose that activity-dependent regulation of LpRs serves as a homeostatic compensatory mechanism to augment the capacity for neuronal lipoprotein uptake in response to chronic elevation of input activity (Figure 7E). Lipoprotein complexes recruited by LpRs are either released by glia or captured from the circulating hemolymph (Figure 7E; Liu et al., 2015, 2017; Palm et al., 2012). This model is supported by our RNA-seq studies, which revealed that a number of lipid-metabolism-related genes are downregulated in the constant light condition, including *FASN1*, *Dgk*, *CG31140*, *GlcAT-S*, *fwd*, and *retm*. LNv transcriptome analysis indicated a strong impact of elevated input activity on lipid metabolism, which may lead to altered lipid homeostasis and increased demand for lipid uptake. *In vivo* studies on activity-induced modifications of lipid homeostasis and trafficking will improve our understanding of the compensatory role of LpR upregulation in neuronal adaptive responses.

Taken together, our studies strongly suggest that neuronal lipoprotein receptors are important components of activity-regulated neural plasticity and adaptive responses. In addition, our transcriptome studies on neuronal-specific responses induced by excessive input activity provide molecular insights for studies related to human epilepsy and seizure disorders and potentially reveal the previously unappreciated role of altered neuronal lipoprotein uptake in neurological disorders associated with the dys-

regulation of lipid homeostasis (Bazinet and Layé, 2014; Müller et al., 2015).

STAR★METHODS

Detailed methods are provided in the online version of this paper and include the following:

- KEY RESOURCES TABLE
- CONTACT FOR REAGENT AND RESOURCE SHARING
- EXPERIMENTAL MODEL AND SUBJECT DETAILS
  - *Drosophila* stocks and culture
- METHOD DETAILS
  - Isolation of larval ventral lateral neurons
  - RNA extraction, library generation and sequencing
  - Bioinformatics analysis
  - Quantitative fluorescence *in situ* hybridization
  - *In vivo* transgenic RNAi screen
  - Immunohistochemistry
  - Calcium imaging
  - Quantification and statistical analysis
- DATA AND SOFTWARE AVAILABILITY

SUPPLEMENTAL INFORMATION

Supplemental information includes seven figures and six tables and can be found with this article online at https://doi.org/10.1016/j.celrep.2018.10.016.

AUTHOR CONTRIBUTIONS

J.Y. and Q.Y. designed the experiments. J.Y. performed RNA-seq library constructions and bioinformatics analyses. J.Y., M.G., C.L, H.S.K., J.R., A.K., U.J., C.S., and Q.Y. performed data collection and analyses. P.D. assisted in the cell isolation step. J.Y. and Q.Y. wrote the manuscript.

DECLARATION OF INTERESTS

The authors declare no competing interests.

REFERENCES

Abruzzi, K.C., Rodriguez, J., Menet, J.S., Desrochers, J., Zadina, A., Luo, W., Tkachev, S., and Rosbash, M. (2011). Drosophila CLOCK target gene characterization: implications for circadian tissue-specific gene expression. Genes Dev. *25*, 2374–2386.

Abruzzi, K.C., Zadina, A., Luo, W., Wiyanto, E., Rahman, R., Guo, F., Shafer, O., and Rosbash, M. (2017). RNA-seq analysis of Drosophila clock and non-clock neurons reveals neuron-specific cycling and novel candidate neuropeptides. PLoS Genet. *13*, e1006613.

Anders, S., Reyes, A., and Huber, W. (2012). Detecting differential usage of exons from RNA-seq data. Genome Res. *22*, 2008–2017.

Anders, S., Pyl, P.T., and Huber, W. (2015). HTSeq: a Python framework to work with high-throughput sequencing data. Bioinformatics *31*, 166–169.

Bailey, A.P., Koster, G., Guillermier, C., Hirst, E.M., MacRae, J.I., Lechene, C.P., Postle, A.D., and Gould, A.P. (2015). Antioxidant role for lipid droplets in a stem cell niche of Drosophila. Cell *163*, 340–353.

Bauer, R., Voelzmann, A., Breiden, B., Schepers, U., Farwanah, H., Hahn, I., Eckardt, F., Sandhoff, K., and Hoch, M. (2009). Schlank, a member of the ceramide synthase family controls growth and body fat in Drosophila. EMBO J. *28*, 3706–3716.

Bazinet, R.P., and Layé, S. (2014). Polyunsaturated fatty acids and their metabolites in brain function and disease. Nat. Rev. Neurosci. *15*, 771–785.

Brown, M.S., and Goldstein, J.L. (1976). Receptor-mediated control of cholesterol metabolism. Science *191*, 150–154.

Bruce, K.D., Zsombok, A., and Eckel, R.H. (2017). Lipid processing in the brain: a key regulator of systemic metabolism. Front. Endocrinol. (Lausanne) *8*, 60.

Chattopadhyaya, B., Di Cristo, G., Higashiyama, H., Knott, G.W., Kuhlman, S.J., Welker, E., and Huang, Z.J. (2004). Experience and activity-dependent maturation of perisomatic GABAergic innervation in primary visual cortex during a postnatal critical period. J. Neurosci. *24*, 9598–9611.

Chen, X., Rahman, R., Guo, F., and Rosbash, M. (2016). Genome-wide identification of neuronal activity-regulated genes in *Drosophila*. eLife *5*, e19942.

Claridge-Chang, A., Wijnen, H., Naef, F., Boothroyd, C., Rajewsky, N., and Young, M.W. (2001). Circadian regulation of gene expression systems in the Drosophila head. Neuron *32*, 657–671.

Cline, H., and Haas, K. (2008). The regulation of dendritic arbor development and plasticity by glutamatergic synaptic input: a review of the synaptotrophic hypothesis. J. Physiol. *586*, 1509–1517.

Cohen, S., and Greenberg, M.E. (2008). Communication between the synapse and the nucleus in neuronal development, plasticity, and disease. Annu. Rev. Cell Dev. Biol. *24*, 183–209.

Darlington, T.K., Wager-Smith, K., Ceriani, M.F., Staknis, D., Gekakis, N., Steeves, T.D., Weitz, C.J., Takahashi, J.S., and Kay, S.A. (1998). Closing the circadian loop: CLOCK-induced transcription of its own inhibitors per and tim. Science *280*, 1599–1603.

Dijkhuizen, P.A., and Ghosh, A. (2005). Regulation of dendritic growth by calcium and neurotrophin signaling. Prog. Brain Res. *147*, 17–27.

Dong, X., Shen, K., and Bülow, H.E. (2015). Intrinsic and extrinsic mechanisms of dendritic morphogenesis. Annu. Rev. Physiol. *77*, 271–300.

Entchev, E.V., Schwabedissen, A., and González-Gaitán, M. (2000). Gradient formation of the TGF-beta homolog Dpp. Cell *103*, 981–991.

Flavell, S.W., and Greenberg, M.E. (2008). Signaling mechanisms linking neuronal activity to gene expression and plasticity of the nervous system. Annu. Rev. Neurosci. *31*, 563–590.

Fujita, N., Nagata, Y., Nishiuchi, T., Sato, M., Iwami, M., and Kiya, T. (2013). Visualization of neural activity in insect brains using a conserved immediate early gene, Hr38. Curr. Biol. *23*, 2063–2070.

Graveley, B.R., Brooks, A.N., Carlson, J.W., Duff, M.O., Landolin, J.M., Yang, L., Artieri, C.G., van Baren, M.J., Boley, N., Booth, B.W., et al. (2011). The developmental transcriptome of Drosophila melanogaster. Nature *471*, 473–479.

Hayashi, H. (2011). Lipid metabolism and glial lipoproteins in the central nervous system. Biol. Pharm. Bull. *34*, 453–461.

Horton, J.D., Goldstein, J.L., and Brown, M.S. (2002). SREBPs: transcriptional mediators of lipid homeostasis. Cold Spring Harb. Symp. Quant. Biol. *67*, 491–498.

Huang da, W., Sherman, B.T., and Lempicki, R.A. (2009). Systematic and integrative analysis of large gene lists using DAVID bioinformatics resources. Nat. Protoc. *4*, 44–57.

Jan, Y.N., and Jan, L.Y. (2010). Branching out: mechanisms of dendritic arborization. Nat. Rev. Neurosci. *11*, 316–328.

Ling, I.F., Gopalraj, R.K., Simpson, J.F., and Estus, S. (2010). Expression and regulation of a low-density lipoprotein receptor exon 12 splice variant. J. Neurochem. *115*, 614–624.

Liu, L., Zhang, K., Sandoval, H., Yamamoto, S., Jaiswal, M., Sanz, E., Li, Z., Hui, J., Graham, B.H., Quintana, A., and Bellen, H.J. (2015). Glial lipid droplets and ROS induced by mitochondrial defects promote neurodegeneration. Cell *160*, 177–190.

Liu, L., MacKenzie, K.R., Putluri, N., Maletić-Savatić, M., and Bellen, H.J. (2017). The glia-neuron lactate shuttle and elevated ROS promote lipid synthesis in neurons and lipid droplet accumulation in glia via APOE/D. Cell Metab. *26*, 719–737.e6.

Lohmann, C., and Wong, R.O. (2005). Regulation of dendritic growth and plasticity by local and global calcium dynamics. Cell Calcium *37*, 403–409.

Love, M.I., Huber, W., and Anders, S. (2014). Moderated estimation of fold change and dispersion for RNA-seq data with DESeq2. Genome Biol. *15*, 550.

Magrané, J., Casaroli-Marano, R.P., Reina, M., Gåfvels, M., and Vilaró, S. (1999). The role of O-linked sugars in determining the very low density lipoprotein receptor stability or release from the cell. FEBS Lett. *451*, 56–62.

Malik, A.N., Vierbuchen, T., Hemberg, M., Rubin, A.A., Ling, E., Couch, C.H., Stroud, H., Spiegel, I., Farh, K.K., Harmin, D.A., and Greenberg, M.E. (2014). Genome-wide identification and characterization of functional neuronal activity-dependent enhancers. Nat. Neurosci. *17*, 1330–1339.

Malpel, S., Klarsfeld, A., and Rouyer, F. (2002). Larval optic nerve and adult extra-retinal photoreceptors sequentially associate with clock neurons during Drosophila brain development. Development *129*, 1443–1453.

Malun, D., and Brunjes, P.C. (1996). Development of olfactory glomeruli: temporal and spatial interactions between olfactory receptor axons and mitral cells in opossums and rats. J. Comp. Neurol. *368*, 1–16.

Mardinly, A.R., Spiegel, I., Patrizi, A., Centofante, E., Bazinet, J.E., Tzeng, C.P., Mandel-Brehm, C., Harmin, D.A., Adesnik, H., Fagiolini, M., and Greenberg, M.E. (2016). Sensory experience regulates cortical inhibition by inducing IGF1 in VIP neurons. Nature *531*, 371–375.

Mauch, D.H., Nägler, K., Schumacher, S., Göritz, C., Müller, E.C., Otto, A., and Pfrieger, F.W. (2001). CNS synaptogenesis promoted by glia-derived cholesterol. Science *294*, 1354–1357.

May, P., Bock, H.H., Nimpf, J., and Herz, J. (2003). Differential glycosylation regulates processing of lipoprotein receptors by gamma-secretase. J. Biol. Chem. *278*, 37386–37392.

McDonald, M.J., and Rosbash, M. (2001). Microarray analysis and organization of circadian gene expression in Drosophila. Cell *107*, 567–578.

Meltzer, S., Bagley, J.A., Perez, G.L., O'Brien, C.E., DeVault, L., Guo, Y., Jan, L.Y., and Jan, Y.N. (2017). Phospholipid homeostasis regulates dendrite morphogenesis in Drosophila sensory neurons. Cell Rep. *21*, 859–866.

Müller, C.P., Reichel, M., Mühle, C., Rhein, C., Gulbins, E., and Kornhuber, J. (2015). Brain membrane lipids in major depression and anxiety disorders. Biochim. Biophys. Acta *1851*, 1052–1065.

Nagarkar-Jaiswal, S., Lee, P.T., Campbell, M.E., Chen, K., Anguiano-Zarate, S., Gutierrez, M.C., Busby, T., Lin, W.W., He, Y., Schulze, K.L., et al. (2015). A library of MiMICs allows tagging of genes and reversible, spatial and temporal knockdown of proteins in Drosophila. eLife *4*, e05338.

Palm, W., Sampaio, J.L., Brankatschk, M., Carvalho, M., Mahmoud, A., Shevchenko, A., and Eaton, S. (2012). Lipoproteins in Drosophila melanogaster–assembly, function, and influence on tissue lipid composition. PLoS Genet. *8*, e1002828.

Parra-Peralbo, E., and Culi, J. (2011). Drosophila lipophorin receptors mediate the uptake of neutral lipids in oocytes and imaginal disc cells by an endocytosis-independent mechanism. PLoS Genet. *7*, e1001297.

Robinson, J.T., Thorvaldsdóttir, H., Winckler, W., Guttman, M., Lander, E.S., Getz, G., and Mesirov, J.P. (2011). Integrative genomics viewer. Nat. Biotechnol. *29*, 24–26.

Rodríguez-Vázquez, M., Vaquero, D., Parra-Peralbo, E., Mejía-Morales, J.E., and Culi, J. (2015). Drosophila lipophorin receptors recruit the lipoprotein

LTP to the plasma membrane to mediate lipid uptake. PLoS Genet. *11*, e1005356.

Ruben, M., Drapeau, M.D., Mizrak, D., and Blau, J. (2012). A mechanism for circadian control of pacemaker neuron excitability. J. Biol. Rhythms *27*, 353–364.

Sieber, M.H., and Spradling, A.C. (2015). Steroid signaling establishes a female metabolic state and regulates SREBP to control oocyte lipid accumulation. Curr. Biol. *25*, 993–1004.

Sin, W.C., Haas, K., Ruthazer, E.S., and Cline, H.T. (2002). Dendrite growth increased by visual activity requires NMDA receptor and Rho GTPases. Nature *419*, 475–480.

Sivachenko, A., Li, Y., Abruzzi, K.C., and Rosbash, M. (2013). The transcription factor Mef2 links the Drosophila core clock to Fas2, neuronal morphology, and circadian behavior. Neuron *79*, 281–292.

Soukup, S.F., Culi, J., and Gubb, D. (2009). Uptake of the necrotic serpin in Drosophila melanogaster via the lipophorin receptor-1. PLoS Genet. *5*, e1000532.

Spiegel, I., Mardinly, A.R., Gabel, H.W., Bazinet, J.E., Couch, C.H., Tzeng, C.P., Harmin, D.A., and Greenberg, M.E. (2014). Npas4 regulates excitatory-inhibitory balance within neural circuits through cell-type-specific gene programs. Cell *157*, 1216–1229.

Sprecher, S.G., Cardona, A., and Hartenstein, V. (2011). The Drosophila larval visual system: high-resolution analysis of a simple visual neuropil. Dev. Biol. *358*, 33–43.

Takemura, S.Y., Karuppudurai, T., Ting, C.Y., Lu, Z., Lee, C.H., and Meinertzhagen, I.A. (2011). Cholinergic circuits integrate neighboring visual signals in a Drosophila motion detection pathway. Curr. Biol. *21*, 2077–2084.

Trapnell, C., Pachter, L., and Salzberg, S.L. (2009). TopHat: discovering splice junctions with RNA-Seq. Bioinformatics *25*, 1105–1111.

Van Hoof, D., Rodenburg, K.W., and Van der Horst, D.J. (2005). Receptor-mediated endocytosis and intracellular trafficking of lipoproteins and transferrin in insect cells. Insect Biochem. Mol. Biol. *35*, 117–128.

Walther, T.C., and Farese, R.V., Jr. (2012). Lipid droplets and cellular lipid metabolism. Annu. Rev. Biochem. *81*, 687–714.

Wang, G.Y., Liets, L.C., and Chalupa, L.M. (2001). Unique functional properties of on and off pathways in the developing mammalian retina. J. Neurosci. *21*, 4310–4317.

Wang, F., Flanagan, J., Su, N., Wang, L.C., Bui, S., Nielson, A., Wu, X., Vo, H.T., Ma, X.J., and Luo, Y. (2012). RNAscope: a novel in situ RNA analysis platform for formalin-fixed, paraffin-embedded tissues. J. Mol. Diagn. *14*, 22–29.

Welte, M.A. (2015). How Brain Fat Conquers Stress. Cell *163*, 269–270.

Wong, R.O., and Ghosh, A. (2002). Activity-dependent regulation of dendritic growth and patterning. Nat. Rev. Neurosci. *3*, 803–812.

Xia, J., Benner, M.J., and Hancock, R.E. (2014). NetworkAnalyst–integrative approaches for protein-protein interaction network analysis and visual exploration. Nucleic Acids Res. *42*, W167–W174.

Xia, J., Gill, E.E., and Hancock, R.E. (2015). NetworkAnalyst for statistical, visual and network-based meta-analysis of gene expression data. Nat. Protoc. *10*, 823–844.

Yin, J., and Yuan, Q. (2015). Structural homeostasis in the nervous system: a balancing act for wiring plasticity and stability. Front. Cell. Neurosci. *8*, 439.

Yu, W., and Hardin, P.E. (2006). Circadian oscillators of Drosophila and mammals. J. Cell Sci. *119*, 4793–4795.

Yuan, Q., Xiang, Y., Yan, Z., Han, C., Jan, L.Y., and Jan, Y.N. (2011). Light-induced structural and functional plasticity in Drosophila larval visual system. Science *333*, 1458–1462.

STAR★METHODS

KEY RESOURCES TABLE

REAGENT or RESOURCE	SOURCE	IDENTIFIER
Antibodies		
rabbit anti-GFP antibody	Abcam	Cat# Ab6556; RRID: AB_305564
anti-Pdf	DSHB	Cat# PDF-C7; RRID: AB_760350
rat anti-HA	Roche	Cat# 11867423001; RRID: AB_10094468
rat anti-Elav	DSHB	Cat# 7E8A10; RRID: AB_528218
Goat anti-rabbit IgG, Alex488+	Thermo Fisher Scientific	Cat# A32731; RRID: AB_2633280
donkey anti-mouse IgG, CY3	Jackson Immuno Research Labs	Cat# 715165150; RRID: AB_2340813
goat anti-rat IgG, Alex 633	Thermo Fisher Scientific	Cat# A-21094; RRID: AB_2535749
Chemicals, Peptides, and Recombinant Proteins		
Bloomington fly food	Genesee	66-112
cornmeal-molasses fly food	Genesee	66-116
Collagenase/ Dispase	Roche	10269638001
liberase I	Roche	05401054001
Schneider's Insect Medium	Sigma	S0146
DNase	QIAGEN	79254
Concanavalin A	Sigma	C5275
30-μm pre-separation filter	Miltenyi Biotech	130-041-407
Critical Commercial Assays		
PicoPure RNA Isolation Kit	Invitrogen	KIT0204
Ovation Single Cell RNA-Seq System	Nugen	0342HV-32
RNAscope Fluorescent Multiplex Kit	Advanced Cell Diagnostics	320850
RNAscope Probe: Dm-LpR2-C1	Advanced Cell Diagnostics	457481
Falcon Culture Slides, Corning	VWR	53106-306
Deposited Data		
RNAseq data	this study	GEO: GSE106930
RNAseq data (larval CNS)	Dr. Susan E. Celniker's lab (Graveley et al., 2011)	ModEncode ID: 4658
RNAseq data (adult LNv)	Dr. Michael Rosbash's lab (Abruzzi et al., 2017)	GEO: GSE77451
CHIP-seq data (CLK)	Dr. Michael Rosbash's lab (Abruzzi et al., 2011)	GEO: GSE32613
Experimental Models: Organisms/Strains		
Pdf-Gal4	Bloomington Drosophila Stock Center	FBst0006899, FBst0006990
UAS-CD8::GFP	Bloomington Drosophila Stock Center	FBst0005137
UAS-Dicer2	Bloomington Drosophila Stock Center	FBst0024650
Pdf-LexA, LexAop-CD8::tdTomato	Dr. YuhNung Jan's lab (Yuan et al., 2011)	N/A
LpR2$^{MI04745\text{-}GFSTF.1}$	Bloomington Drosophila Stock Center	FBst0060219
UAS-Rab5-GFP	Bloomington Drosophila Stock Center	FBst0043336
UAS-shi^{K44A}	Bloomington Drosophila Stock Center	FBst0005811
LpR1$^{-/-}$ (Df(3R) lpr1)	Bloomington Drosophila Stock Center	FBst0044236
LpR2$^{-/-}$ (Df(3R) lpr2)	Bloomington Drosophila Stock Center	FBst0044233
LpR1/2$^{-/-}$ (Df(3R) lpr1/2)	Dr. Joaquim Culi's lab (Parra-Peralbo and Culi, 2011)	N/A
UAS-LpR1D	Dr. Joaquim Culi's lab (Parra-Peralbo and Culi, 2011)	N/A
UAS-LpR2F-HA	Dr. Joaquim Culi's lab (Parra-Peralbo and Culi, 2011)	N/A
LpR1 RNAi^{27249}	Bloomington Drosophila Stock Center https://bdsc.indiana.edu/	FBst0027249
LpR2 RNAi^{54461}	Bloomington Drosophila Stock Center	FBst0054461
SREBP RNAi^{34073}	Bloomington Drosophila Stock Center	FBst0034073

(Continued on next page)

Continued

REAGENT or RESOURCE	SOURCE	IDENTIFIER
schlank RNAi[29340]	Bloomington Drosophila Stock Center	FBst0029340
UAS-GCaMP6s	Bloomington Drosophila Stock Center	FBst0042746
Software and Algorithms		
HTSeq	(Anders et al., 2015)	N/A
R	R-project	N/A
IGV	(Robinson et al., 2011)	N/A
DESeq2	(Love et al., 2014)	N/A
DAVID 6.7	(Huang da et al., 2009)	N/A
DEXSeq	(Anders et al., 2012)	N/A
Imaris v8.0	Imaris Software	N/A
GraphPad Prism v.6	GraphPad Software	N/A
Tophat	(Trapnell et al., 2009)	N/A

CONTACT FOR REAGENT AND RESOURCE SHARING

Further information and requests for resources and reagents should be directed to and will be fulfilled by the Lead Contact, Quan Yuan (quan.yuan@nih.gov).

EXPERIMENTAL MODEL AND SUBJECT DETAILS

Drosophila stocks and culture

Fly stocks are maintained in the standard cornmeal-based fly food in a 25°C incubator with humidity control. For developmentally staged larvae, embryos with the desired genotypes were collected on plates containing grape juice agar supplemented with yeast paste. 1st instar larvae hatched within a 2 hour time window. Larvae are cultured in either the light and dark (LD) condition with a 12 hour light:12 hour dark light schedule; or in the constant light (LL) condition under 24hour light. Unless otherwise noted, all larvae were collected between ZT1-ZT3 (ZT: zeitgeber time in a 12:12 h light dark cycle; lights-on at ZT0, lights-off at ZT12).

METHOD DETAILS

Isolation of larval ventral lateral neurons

Embryos expressing *Pdf-Gal4 > UAS-CD8::GFP* were collected and cultured under LD and LL conditions. Brains from late 3rd instar larvae (120hr AEL) were dissected with ventral nerve cord (VNC) removed. For each biological replicate, approximately 200 brains were dissected for LNv neuron isolation.

Brain dissociation protocol was modified from previously published methods (Ruben et al., 2012; Takemura et al., 2011). Brains were transferred to clean dish containing cold DPBS and were cut into smaller pieces by needles. Then they were transferred into a 2 mL microcentrifuge tube and incubated in 0.8 mL protease mixture (Collagenase/ Dispase [1 mg/ml] and liberase I [0.1 Wünsch units/ml], Roche, 10269638001 and 05401054001) for 40 min at 25°C. To facilitate cell dissociation, tissue was triturated until most tissue was dissociated to single cells. Schneider's Insect Medium (Sigma, S0146) with antibiotics (Penicillin-streptomycin-kana-mycin, 100 μg/ml) and 5% Fetal Bovine Serum was added to neutralize proteinase digestion. Cells were then strained through a 30-μm pre-separation filter (Miltenyi Biotech, 130-041-407), pelleted by centrifugation at 600 g for 5 mins at 10°C and then washed one time with DPBS. Cells were resuspended in 1ml DPBS and DAPI was added to stain the dead cells. 200-400 cells were yielded from each FACS sorting and directly lysed in the RNA extraction buffer. Samples were then incubated at 42°C for 30 min and stored at −20°C for RNA extractions.

RNA extraction, library generation and sequencing

RNA was extracted with Arcturus PicoPure RNA extraction kit (Invitrogen, KIT0204) with added DNase (QIAGEN, 79254) for removal of the genomic DNA. RNA-seq libraries were generated using Ovation Single Cell RNA-Seq System (Nugen, 0342HV-32) following the standard protocol. The reverse transcription was performed by using customized fly primer mix (Nugen designed fly primers: 2.5 μl, oligo dT: 1.3 μl, buffer: 6.2 μl).

Barcoded libraries were sent to NHLBI DNA core facility for pair-end sequencing. Reads passing Phred quality score Q30 were collected. Approximately 20-30 millions of paired-end reads were yielded for each library with 50bp or 75bp length for each end.

Bioinformatics analysis

We mapped pair-end reads to the FLYBASE *Drosophila melanogaster* reference genome r6.05 (ftp://ftp.flybase.net/genomes/Drosophila_melanogaster/dmel_r6.05_FB2015_02/) with the gapped aligner Tophat (Trapnell et al., 2009) using the default setting. Reads uniquely aligned to the exon region were counted by HTSeq (Anders et al., 2015). The annotated reference gtf file and gff file are Ensembl BDGP6.82 version. Reads mapped to each RNA type were calculated using customized Perl scripts (http://history.perl.org/PerlTimeline.html). Reads mapped to mRNA genes were used for further analysis.

The values for Pearson's coefficients between each library were calculated with raw mRNA reads and the correlation figure were generated using R scripts. FPKM units (Fragments Per Kilobase of exon per Million reads mapped) were calculated with raw mRNA reads using customized scripts written in Perl. To visualize the level of transcripts in the sequencing libraries, bigwig visualization files were made from bam files and were plotted using the integrated genome browser (IGV) (Robinson et al., 2011). In Figures 1 and S2, IGV images were generated using one presentative library from each condition (LD: 6.8 million reads; LL: 6.9 million reads) or brain (5.4 million reads) with comparable number of total mRNA reads.

We performed principal component analyses (PCA) on DESeq2 normalized read counts of all samples to compare gene expression under different conditions using the 'prcomp' function in R. The 500 top-ranked genes based on their variations were selected for PCA calculation.

Statistical analyses of differential gene expression was carried out with the DESeq2 package in the R environment (Love et al., 2014). A local smoothed dispersion fit was selected for dispersion estimation. To reduce false positive DE profiles, auto independent filtering was used to filter out genes with low average counts. DE genes fit the following criteria: 1. Adjusted p value (FDR) < 0.1; 2. the absolute value of Log2 fold change between LD and LL condition > 1; 3. genes passed the independent filtering (Mean normalized counts crossing libraries > 336).

We generated the MA Plot to show the log2 fold changes attributable to a given variable over the mean of normalized counts for all detected genes. Z-score of the DE genes were calculated based on variance stabilizing transformed value from DESeq2. Heatmaps were produced from normalized expression data using heatmap.2 in gplots package for R. Gene ontology analysis was generated by DAVID 6.7 version (Huang da et al., 2009). Network analysis was generated by NetworkAnalyst (Xia et al., 2014, 2015).

RNA-seq data for *Drosophila* 3rd instar larval central nervous system (CNS) were downloaded from ModEncode (ID-4658). Exons mapped to LpR1 and LpR2 genes were visualized using the integrated genome browser (IGV). One representative library from each condition of LNv and CNS were used for generating IGV exon images. LD: 7.2 million reads; LL: 6.9 million reads; CNS: 21 million reads.

Quantitative fluorescence *in situ* hybridization

Quantitative fluorescence *in situ* hybridization (qFISH) was performed using a RNAscope Fluorescent Multiplex Kit (Advanced Cell Diagnostics, 320850)(Wang et al., 2012). Customized C1 DNA oligonucleotide probes were designed for *LpR2* by Advanced Cell Diagnostics (Cat: 457481). FISH experiments were performed on acutely dissociated larval brain cells. After proteinase treatment, media neutralization and centrifuge, cells were resuspended in 30 μL Schneider's Insect Medium and transfer onto chambered cell culture slides (VWR, 53106-306), which were pretreated with 0.25mg/ml Concanavalin A (Sigma). There are four LNvs in each brain lobe and about 20% of the dissociated LNvs were recovered. After 10min at room temperature, extra solution was removed from the slides. Adhered cells were then fixed in 4% paraformaldehyde in PBS for 10 min and then washed with PBST twice. Subsequent fluorescent *in situ* hybridization steps were performed following manufacture's protocol for adherent cells. LNvs were identified by either Pdf enhancer driving GFP expression or by immunostaining using the anti-PDF antibody.

In vivo transgenic RNAi screen

Pdf-gal4, *UAS-Dicer2; UAS-CD8::GFP line* was crossed with transgenic RNAi lines targeting candidate molecules. Larvae brains were dissected at wandering late 3rd instar stage (120hr AEL). Brains were fixed with 4% PFA/PBS and followed by 3 rounds of PBST wash. After mounting, at least 10 brains were imaged for the assessment of dendrite phenotype.

Immunohistochemistry

Larval brains collected at specific developmental stages were dissected and fixed in 4% PFA/PBS at room temperature for 30 min, followed by washing in PBST (0.3% Triton X-100 in PBS), and incubating in the primary antibody overnight at 4°C. On the next day, brains were washed with PBST and incubated in the secondary antibody at room temperature for 1 hour before final washes in PBST and mounting on the slide with the anti-fade mounting solution. Primary antibodies used were rabbit anti-GFP antibody (Abcam, Ab6556, 1: 200), mouse anti-PDF (DSHB PDF C7, 1:10), rat anti-HA (Sigma, 11867423001, 1:200) and rat anti-Elav (DSHB, 7E8A10, 1:10). Secondary antibodies used were goat anti-rabbit Alex488+ (Invitrogen, A32731), donkey anti-mouse CY3 (Jackson Immuno Research Labs, 715165150), goat anti-rat Alex 633 (Invitrogen, A-21094).

Calcium imaging

Late 3rd instar larvae expressing *Pdf*-Gal4 driving *UAS-GCaMP6s* were used for calcium imaging experiments as described (Yuan et al., 2011). Imaging was performed on a Zeiss LSM 780 confocal microscope equipped with a Coherent Vision II multiphoton laser. Larval brain explants were dissected in the external saline solution (120 mM NaCl, 4 mM MgCl$_2$, 3 mM KCl, 10 mM NaHCO$_3$, 10 mM

Glucose, 10 mM Sucrose, 5 mM TES, 10 mM HEPES, 2 mM Ca^{2+}, PH 7.2) and maintained in a chamber between the slide and cover-glass and imaged with a 40x water objective using 920 nm excitation for GCaMP signals. GCaMP6s signals were collected at 100 ms/frame for 2000 frame during each recording session with the optic resolution at 256 × 90. Light stimulations of 100 ms duration were delivered using a 561nm confocal laser controlled by the photo bleaching program in the Zen software. The laser power was set at 10%. GCaMP6s signals at the axonal terminal region of LNvs were recorded and analyzed. Average GCaMP6s signals of 20 frames before light stimulation was taken as F0, and ΔF (F-F0)/F was calculated for each time point. The average value of ΔF/F for individual brain samples were used to generate the average traces of calcium transients. The shaded area represents the standard-error of mean. The sample number n represents number of individual animals subjected to the optical recordings.

Quantification and statistical analysis

For LNv dendrite volume quantification, images of LNvs were obtained from fixed whole-mount larval brains using a 40x oil objective. Serial optic sections of 0.2-0.50 μm thickness were taken on a Zeiss-700 or Zeiss-880 Aryscan confocal microscope and processed by Imaris 3D image visualization software. The imaging setting were kept consistent in all experiments. For 3D reconstruction and quantification of LNv dendrites, the surface module of the Imaris (Bitplane) software was used to detect the GFP intensity on dendritic arbors and reconstruct the surface that encamps the whole dendritic tree. The dendrite volume was exported from Imaris into Excel and used for calculations.

For the qFISH experiment, numbers of dots generated by the *LpR2* probe in each LNv neuron were manually counted for quantifications. For quantifications of the levels of *MiMIC-LpR2-EGFP* expression, LNv somas were reconstructed with Surface module based on anti-PDF signal. The absolute intensity and volume of GFP signal in reconstructed somatic areas were exported from Imaris. The mean GFP intensity in the soma was calculated by total intensity divided by volume. The relative intensity was normalized by the arithmetic mean intensity (from Zen software) of each image's background.

Graphing and statistics analysis of the quantifications were performed using Graphpad Prism V6.0. For statistical analyses between two groups of samples, two-tailed unpaired Student's t test was performed; for experiments with more than two groups, one-way ANOVA analysis followed by multiple comparisons Tukey post hoc test was performed. Exact value of sample number n, the statistical testes used and the confidence intervals and the precision measures for individual experiments are included in the figure legends. Most quantitative data are presented as bar plot overlaid with dot plot; bar plot shows the mean (height of bar) and SEM (error bars); dot plot displays individual data points. Calcium imaging data in Figure 7C are presented as line graph showing the mean ± SEM as indicated. n represents the number of libraries in Figure 3B; n represents number of larvae in Figures 3C, 5D, 6B, 6D, 7D, and S5B; n represents the number of dissociated LNvs in Figure 4. Statistical significances were assigned as: $*p < 0.05$, $**p < 0.01$, $***p < 0.001$, ns: not significant.

DATA AND SOFTWARE AVAILABILITY

The accession number for the LNv specific RNA-seq dataset reported in this paper is GEO: GSE106930.